

# **Mars global MHD predictions of magnetic connectivity between the dayside ionosphere and the magnetospheric flanks**

Michael W. Liemohn, Yingjuan Ma

Center for Planetary Sciences, AOSS Department, University of Michigan, Ann Arbor, MI

Rudy A. Frahm

Southwest Research Institute, San Antonio, TX

Xiaohua Fang, Janet U. Kozyra, Andrew F. Nagy

Center for Planetary Sciences, AOSS Department, University of Michigan, Ann Arbor, MI

J. David Winningham, James R. Sharber

Southwest Research Institute, San Antonio, TX

Stas Barabash, Rickard Lundin

Swedish Institute of Physics, Kiruna, Sweden

Submitted to *Space Science Reviews*

## **Running Title:**

LIEMOHN ET AL.: MARS M-I COUPLING

**Abstract.** Atmospheric photoelectrons have been observed well above the ionosphere of Mars by the ASPERA-3 ELS instrument on Mars Express. To systematically interpret these observations, field lines from two global MHD simulations were analyzed for connectivity to the dayside ionosphere (allowing photoelectron escape). It is found that there is a hollow cylinder behind the planet from 1-2  $R_M$  away from the Mars-Sun line that has a high probability of containing magnetic field lines with connectivity to the dayside ionosphere. These results are in complete agreement with the ELS statistics. It is concluded that the high-altitude photoelectrons are the result of direct magnetic connectivity to the dayside at the moment of the measurement, and no extra trapping or bouncing mechanisms are needed to explain the data.

## 1. Introduction

*Frahm et al.*, [2006a, b] have reported observations of atmospheric photoelectrons well above the ionosphere of Mars by the ASPERA-3 electron spectrometer (ELS) instrument [*Barabash et al.*, 2004] on Mars Express (MEX) [*Chicarro et al.*, 2004]. These high-altitude measurements reveal the characteristic photoelectron primary production peaks in the 20-30 eV energy range in a small angular width looking back toward the planet. These electrons are created in the dayside ionosphere, yet they are seen thousands of kilometers above the planet, well into the flanks of Mars' induced magnetosphere. *Frahm et al.* [2006a] believe that this electron signature (the 20-30 eV number flux peaks) sufficiently identifies them as atmospheric photoelectrons because nothing else is known to create such an energy spectrum. They are not observed everywhere, but rather in limited spatial regions around the planet, namely a slowly-expanding cone of 1-2  $R_M$  in radius on the flanks and just behind Mars [*Frahm et al.*, 2006b]. Anecdotally, the observation of these photoelectrons has been shown to be associated with direct magnetic connection between the measurement location and the dayside ionosphere [*Liemohn et al.*, 2006]. The electrons were thought to simply flow out along an open or draped field line from the dayside ionosphere directly to MEX.

The question still remains of whether this conclusion from a few case studies is the dominant mechanism for allowing the observation of atmospheric photoelectrons high above the ionosphere of Mars. That is, direct magnetic connection with the dayside ionosphere is one scenario, but other possibilities exist. One such process is trapping on closed field lines associated with the strong crustal magnetic field anomalies. Such trapping regularly occurs at Earth [e.g., *Swartz et al.*, 1975; *Lejeune and Wörmsler*, 1976; *Khazanov and Liemohn*, 1995]. Downward-flowing flux spikes have been observed by Mars Global Surveyor across the nightside of Mars, occurring at the “cusps” of the strong crustal field regions [*Mitchell et al.*, 2001]. These precipitating electrons are presumably of solar wind origin, but they could also be photoelectrons, trapped during the day and dumped into the ionosphere sometime during the

night. At Earth, trapped photoelectrons slowly precipitate throughout the night, contributing to the thermal balance of the ionospheric F layer [e.g., *Nagy and Banks, 1970; Swartz et al., 1975; Khazanov et al., 1998, 2000*]. The MEX observations of high-altitude photoelectrons could be related to trapping within mini-magnetospheres. Another scenario is that these atmospheric photoelectrons are bouncing along draped interplanetary magnetic field (IMF) lines, and that there are some preferential locations where they can be observed flowing away from the planet and others where they should be seen flowing towards Mars.

The present study addresses this question to determine the true transport scenario for these electrons. Specifically, this study addresses the first hypothesis of direct magnetic connection between the dayside ionosphere and the locations where MEX statistically observes these particles. The magnetohydrodynamic (MHD) model of *Ma et al. [2004]* is used for this investigation, extracting many field lines from two simulation results to examine the magnetic topology around Mars. In brief, it is found that direct magnetic connection is fully capable of explaining the Mars Express high-altitude photoelectron observations, and more complicated methods of transport are not necessary.

## **2. Numerical Approach**

*Ma et al. [2002, 2004]* provide a detailed description of the MHD model employed in the present study. Briefly, it solves the non-ideal MHD equations in dimensionless conservative form, using multiple continuity equations for the various ion species ( $H^+$ ,  $O^+$ ,  $O_2^+$ , and  $CO_2^+$ ), and single-fluid versions of the momentum and energy equations. The solution, obtained on a non-uniform spherical grid, uses the second-order accurate numerical scheme of *Powell et al. [1999]*. Thermospheric parameters are taken from the model of *Bougher et al. [2001]*, and the strong crustal fields are included with the spherical harmonic model of *Arkani-Hamed [2001, 2002]*. A nominal Parker spiral interplanetary magnetic field and average solar wind flow conditions are assumed for the upstream conditions in the simulations, in agreement with the typical values reported by *Luhmann and Brace [1991]*. The MHD model is run until a steady-state solution is

achieved. This is justified because of the fast transit times of photoelectrons in the Mars space environment. For example, a 25 eV electron has a speed of nearly 3000 km/s, and can therefore, if directed upward, leave the Mars ionosphere in much less than a second and travel many Mars radii distance away from the planet in just a few seconds. The temporal change in the global magnetic topology can therefore be neglected for this application. Note that these are the same conditions used in the simulations discussed by *Ma et al.* [2004] and *Liemohn et al.* [2006], and additional details of the configuration set up are discussed there.

Results from two simulations are examined in this study. The only difference between these two simulations is the subsolar longitude of Mars:  $0^\circ$  and  $180^\circ$ . Because the strong crustal field region is concentrated around  $180^\circ$  east longitude [e.g., *Acuña et al.*, 1998; *Connerney et al.*, 2001], these two choices represent the extremes of the influence of the crustal fields on the magnetic topology of near-Mars space. The  $0^\circ$  subsolar longitude case has the strongest crustal fields on the nightside, and therefore their effect on magnetic field connection to the dayside ionosphere is minimized. In the  $180^\circ$  subsolar longitude case, the effect is maximized, and the existence of open magnetic field lines (connected to the planet and to the IMF) is likely.

*Ma et al.* [2004] has already presented and discussed the general magnetic topology of the two MHD simulation results to be examined in this study. To summarize, IMF draping dominates the magnetic field configuration in both cases, but the strong crustal field sources create localized regions of closed field lines (mini-magnetospheres). Some of these field lines, especially those on the nightside, can extend thousands of kilometers above Mars. On the dayside, the closed field line regions are, in general, contained by the IMF, and the magnetic pile-up region around Mars [e.g., *Luhmann and Brace*, 1991; *Crider et al.*, 2002; *Vennerstrom et al.*, 2003] is pressed outward in some places, but only by a few hundred kilometers at most [*Ma et al.*, 2004].

In order to examine the magnetic connection between the dayside ionosphere and the MEX observation locations of high-altitude photoelectrons, many magnetic field lines were extracted from each of these simulations. The field line traces began from a grid in the  $x=0$

(terminator) plane. This starting point grid extended from 200 km altitude out to 6600 km (near  $2 R_M$ ) altitude, with an extraction every 200 km altitude in this range. This was done every  $10^\circ$  around the planet in the y-z terminator plane. Thus, there were 33 altitude starting points at 36 clock angle locations, resulting in 1188 field lines extracted from each simulation.

The field lines are designated as connected to the dayside ionosphere when they cross below an altitude of 300 km at daytime local times (i.e., 06-18 LT). This is roughly the altitude when the ionospheric density is 1% of the peak value (see Figure 13.10 of *Schunk and Nagy* [2000], taken from *Hanson et al.* [1977]). Selection of this altitude means that this study cannot easily differentiate between open magnetic field lines and draped magnetic field lines that pass below this threshold. This is unfortunate, but this information the nature of the MHD results already made this distinction difficult. That is, the assumed grid resolution in the MHD simulations lowers the fidelity of the field line tracing through the ionosphere. This is because the inner boundary condition for the magnetic field is specified at the average crustal field vector for each horizontal cell face at 100 km altitude (the lower boundary of the MHD model). The cells are roughly 100 km wide; therefore, resolving small-scale structures in the crustal fields, such as cusp-like features, is problematic. However, it is precisely at these cusps where reconnection between the crustal and interplanetary fields might occur. Resolution of the issue of open or draped field line topology is not necessary for the present study, however. The only thing that matters is magnetic connection to the dayside ionosphere, and a 300 km altitude sphere has been chosen for this designation. Note that this means the entire ring of extracted field lines beginning at 200 km altitude in the terminator plane are designated as having dayside ionospheric connection.

### **3. MHD Modeling Results**

Figure 1 shows a few example 3-D field line traces extracted from the MHD results with 180E longitude at local noon. In Figures 1a and 1b are plotted lines that start somewhere along a semicircle in the northern hemispheric terminator plane at 1000 km, seen from the front and from

the side. The color of the field lines shows the local magnetic field magnitude. Figures 1c and 1d are similar plots, but for field lines starting at 2000 km altitude in the terminator plane. The plotting of each field line stops when it reaches either 300 km altitude or the boundary of the plotting domain (into Mars' atmosphere to 300 km altitude, to the side to  $Y = \pm 3 R_M$ , behind the planet to  $X = -5 R_M$ , or up or down to  $Z = 0$  or  $+1.5 R_M$ ).

It is seen that most of the lines in Figures 1a and 1b (1000 km starting altitude) connect to the dayside ionosphere, while very few of those in Figures 1c and 1d (2000 km starting altitude) show such a connection. As noted above, it is unclear whether these field lines are connected to the planetary crustal field sources, or are simply draped IMF field lines. For the northern hemisphere, shown here, it is assumed that most are draped IMF lines because of the weak crustal sources at northern latitudes. Note that for the connected field lines,  $B$  is seen to vary much more along the field line than for the unconnected field lines.

For comparison with the MEX data, it is useful to identify where the field lines with dayside ionospheric connectivity go in their paths around Mars. Figure 2 is an illustration of this, showing the locations of the dayside-ionosphere-connected field lines as they pass through the  $x=0$ ,  $-2$ , and  $-5 R_M$  planes. The two columns show the dayside-connected field line locations for the 2 simulations (180E at noon on the left, 0E at noon on the right).

Several prominent features are worth noting in Figure 2. First, many of the field lines pass through a ring 1-2  $R_M$  from the  $-x$  axis. Across the northern hemisphere, these are most likely draped IMF field lines passing through the inner edge of the magnetic pile-up region in front of Mars. In the southern hemisphere, the abundance of field lines in this ring is much larger in Figures 2a, 2c, and 2e (180E at local noon) than in Figures 2b, 2d, and 2f (0E at local noon). This implies that many of them in this  $z < 0$  region are open field lines, i.e., the field lines that are connected to one of the planet's crustal sources and to the IMF.

There is the possibility that the center of this cylinder of connectivity is also connected to the dayside ionosphere. The selection of the terminator plane for the beginning of the field line traces means that the patterns in Figure 2 could be reflecting the region of high magnetic field

intensity and not necessarily the entire region of dayside ionospheric connection. This is most likely not the case, however. The field line extractions include a ring of starting points at 200 km altitude, and none of these field lines in either of the simulations escapes beyond the ionosphere of Mars. Therefore, if there were field lines from very close to the  $-X$  axis with dayside ionospheric connection, they would have to pass through a portion of the nightside ionosphere/thermosphere, where the numerous Coulomb collisions would seriously degrade the flux intensities. This would make a high-altitude observation difficult and unlikely. To confirm this, additional field line extractions were conducted with starting points distributed in the  $X=-2 R_M$  plane. The resulting patterns of dayside ionospheric connection are very similar to those presented in Figure 2. While it could be that the MHD model is incorrectly tracking the exact field line paths at low altitudes, it is believed that the field lines within the cylinder are not populated by atmospheric photoelectrons.

Another feature is the presence of several field lines along the  $+y$  axis in both sets of plots. These are draped field lines that extend into the magnetosheath, yet still have a connection to the dayside ionosphere. These field lines, in general, have slightly higher closest approach altitudes within the ionosphere, but still pass within 300 km altitude of the planet.

A final feature of these plots is the presence of field lines far out on the  $-y$  axis in Figures 2d-2f. These are locations beyond the bow shock, but on field lines that form an S shape in the  $x-y$  plane, crossing the bow shock on the dawn side, continuing back a bit in the magnetosheath, and then sweeping sunward again to drape around the dayside ionosphere. They cross the terminator plane 3 times in their trace around Mars. Two examples of such field lines are shown in Figure 3.

The locations of  $y-z$  plane crossings at various  $x$  distances can be quantified for direct comparison with the statistical results of *Frahm et al.* [2006b]. To do this, a cylindrical grid was defined, transforming the  $y-z$  plane location into polar coordinates, measured as  $\rho$  (distance from the  $x$  axis) and  $\phi$  (counterclockwise angle measured from the  $+y$  axis). The cylindrical grid was defined by dividing the  $x$  distance and the radial distance  $\rho$  into  $0.1 R_M$ -wide bins, and dividing

the  $\phi$  angle into 24 equal bins around its  $2\pi$  extent. If one or more field lines with dayside ionospheric connectivity passed through a particular bin, that bin was assigned a value of 1. If not, the bin was given a zero value. These values were then averaged around each  $\phi$  ring, producing an array of fractions in the  $x$ - $\rho$  plane of the amount of dayside ionospheric connectivity for that cylindrical location.

The results of this exercise are shown in Figure 4, for the cases of 180E and 0E longitude at local noon (Figures 4a and 4b, respectively). The color scale is logarithmic in order to highlight the smaller fractions in the magnetosheath and upstream solar wind. Of course, the dayside ionosphere has fractions at or near unity, as expected. However, it is seen that there is a channel (actually, a cylinder) of high fractions behind Mars located 1 to 2  $R_M$  away from the  $x$  axis. The fractions are very high, with values above 0.5 even 4  $R_M$  and 2  $R_M$  downtail (in Figures 4a and 4b, respectively). At larger  $\rho$  values, in the magnetosheath, the fractions can still be as high as 0.1 in some places. Even in the solar wind upstream of the bow shock, there are non-zero fractions present in both simulation results (from the S-shaped field lines in the  $x$ - $y$  plane).

These plots in Figure 4 clearly demark the regions of high probability for a spacecraft to be located on a field line with direct magnetic connection to the dayside ionosphere, and therefore for the electron detector onboard the satellite to measure atmospheric photoelectrons far away from their source region. A comparison with high-altitude measurements of atmospheric photoelectrons is now possible.

#### **4. Comparison with high-altitude photoelectron observations**

One such spacecraft with a good orbit and appropriate detector is MEX. The eV-energy-range electron detector on MEX, ELS, consists of a collimator followed by a standard top-hat electrostatic analyzer, with a micro channel plate and anode ring below this. The anode is divided into 16 sectors of  $22.5^\circ$ , making the field of view  $360^\circ$  with a  $4^\circ$  collimator window. The energy range extends from below an electron volt to  $\sim 20$  keV, with a  $\Delta E/E$  of 0.08.

At high altitudes, ELS is oriented on the MEX satellite in such a way that anode sector 3 is in the Sun-looking direction. Thus, *Frahm et al.* [2006b] chose to examine the data in this sector in their statistical analysis of high-altitude photoelectron observations. By looking for the primary production peaks from the photoionization of CO<sub>2</sub> by 30.4 nm solar photons (in the 20-30 eV energy range), they were able to determine if a given energy spectrum from this anode sector contained an atmospheric photoelectron signature. Data were considered throughout most of 2004, and so the analysis included tens of thousands of energy spectra across a wide range of near-Mars space.

Figure 5a presents a plot of the fraction of observations that contained atmospheric photoelectrons in sector 3, shown in cylindrical coordinates, like Figure 4. It is seen that the dayside ionosphere has very high fractions, but there are also high fractions, approaching unity, in a channel (cylinder) roughly 1 to 2 R<sub>M</sub> from the x axis extending downtail. This result is in excellent agreement with the MHD simulation results of direct dayside ionospheric connection shown in Figure 4.

Also shown in Figure 5a is the region of ELS data coverage included in the *Frahm et al.* [2006b] study. While the sampling is not uniform within this region, most x-ρ grid points within this region have tens (and often hundreds) of sector 3 spectra included in the analysis.

The “excellent” comparison with Figure 4 is qualitative, however. Two main reasons account for this caveat. Firstly, Mars rotates about its axis each day, exposing a different configuration of crustal magnetic field sources to the magnetic pile-up region. Secondly, the solar wind is also varying throughout the day. Therefore, neither of the plots in Figure 4 is truly analogous to the statistical results. While the latter effect requires additional simulations to investigate, two points lend validity to this study without such additional numerical experiments. The first is the choice of average solar wind and IMF conditions for these simulations, which should yield a “typical” solar wind interaction with Mars. The second is that the results are averaged in azimuth in the y-z plane, which means that different IMF clock angles will not affect the results. That is, the locations of dayside ionospheric connectivity will rotate around in the y-

z plane with changes in the IMF  $B_y$  and  $B_z$  components, but such rotation will not change the  $\phi$ -averaged fractions.

To crudely take into account the former factor (accounting for Mars' daily rotation), the results from the 2 simulations, which represent the 2 extremes of crustal field influence on the magnetic field topology around Mars, can be simply averaged together. Figure 5b presents the results from this averaging step. These results are now comparable to the statistical results of *Frahm et al.* [2006b], shown in Figure 5a. Both plots are in cylindrical coordinates and plotted with a linear color scale to highlight the region of MEX observations. While the agreement is not perfect, the existence of the high-fraction channel extending into the Mars magnetotail roughly 1 to  $2 R_M$  from the x axis is clearly visible in both plots.

One major difference between the two plots in Figure 5 is at and just behind the terminator ( $x=0$  to  $-1$ ), where the observation-based fractions are low but the MHD-based fractions are high. While the true reason for this discrepancy is unknown, the likely explanation is an observational bias due to the use of sector 3 for the automatic identification routine. In this region, MEX sometimes (on about half of the orbits) changes its orientation relative to the Sun and Mars so that the cameras face the planet surface. In addition, the magnetic field line is often not parallel to the x axis in this region, but rather curved, and so the field-aligned flows are directed into sector 4 or 5 rather than sector 3. Because of the dramatic magnetic field decrease between the photoelectron source region and this flank region, the photoelectron source cone is probably  $20^\circ$  or less in pitch angle (i.e., smaller than a single sector width). So, the photoelectron stream could simply be striking a different anode sector. Another complication is that even when sector 3 is Sun-looking, the ELS detector plane is parallel to the x-y plane, and any tilt of the magnetic field out of the x-y plane reduces the observed pitch angle extent seen by ELS. The first pitch angles to be lost because of this tilt are those near  $0^\circ$  and  $180^\circ$ , i.e., the source cone where the photoelectrons are located. As seen in Figure 1, the field lines between  $x=0$  and  $x=-1 R_M$  are often not parallel to the x axis, as they are farther downtail, but rather they are pointed in many different directions. So, this effect also acts to reduce the chances of observation in this

window of the x axis. Thus, sector 3 is an unreliable sector for photoelectron detection in this particular spatial region near Mars, and other sectors must be examined, depending on the spacecraft and magnetic field orientation. That is, sector 3 simply might not have seen the atmospheric photoelectrons in this spatial region.

On the dayside, the observations are near the source region of the atmospheric photoelectrons. Therefore, the pitch angle distribution is nearly isotropic and the photoelectrons often appear in many (or all) ELS sectors. So, even though the field lines point in all directions here as well, the observation fraction for sector 3 is still high.

A final note on the data-model comparisons is that while there are many ELS sector 3 energy spectra recorded while MEX was in the magnetosheath and unshocked solar wind. That is, in Figure 5a, compare the ELS coverage region encompassed by the black dotted line with the statistical locations of the magnetopause and bow shock shown by the blue lines. The occurrence fractions of atmospheric photoelectron observations are essentially zero in these regions. Again, this is because the statistics are based on an examination of ELS sector 3 observations, which (at high altitudes) requires a magnetic field parallel to the x axis (or an isotropic distribution) for any chance of detection. Therefore, it is not surprising that the ELS statistics have fractions at or near zero in these regions. Note that the *Frahm et al.* [2006b] analysis of sector 3 photoelectron measurements is a pilot study and will be followed up with a more detailed investigation of additional sectors.

## **5. Discussion and Conclusions**

In this study, the question has been systematically addressed of how atmospheric photoelectrons can be seen with such high probability thousands of kilometers away the dayside ionosphere of Mars. To do this, the near-Mars magnetic topology was simulated with an MHD model, and extracted many field lines from the results. These field lines were checked for connection to the dayside ionosphere, and a similar "statistical analysis" of the simulation results of atmospheric photoelectron probabilities was conducted. The resulting maps are in excellent

agreement with the observation-based statistics of the electron spectrometer on Mars Express, and the main discrepancies between the data and the model results can be readily explained.

The observation of atmospheric photoelectrons far from the dayside ionosphere can be a powerful tool for interpreting the solar wind interaction with Mars. It reveals direct magnetic connection with the dayside ionosphere and upper atmosphere, and therefore is an indicator of where to look for very-low-energy (i.e., thermal) escaping planetary ions (those streaming along the field line). In fact, atmospheric photoelectron intensities should be closely related to ionospheric temperatures (photoelectron energy deposition is a major heat source) and therefore the flux of these electrons could be used as a proxy for the flux of escaping ions. This issue of photoelectron flux at high altitudes has not been addressed in this study; only the magnetic connection to the dayside ionosphere is being examined. *Liemohn et al.* [2006] calculated such fluxes and discuss many of the processes affecting these fluxes. Another feature of high-altitude photoelectron observations is that their location will vary with changes in the solar wind and IMF, and therefore they can be used to deduce the upstream conditions, even in the absence of a direct measurement.

To address the question posed in the Introduction, the answer is that no “fancy” trapping or bouncing mechanisms are needed to get photoelectrons to the high altitudes where ELS observes them. All that is needed is a simple and direct magnetic connection between the observation location and the dayside ionosphere of Mars.

**Acknowledgments.** The authors would like to thank support for this research by NASA under grants NASW-00003, NAG5-10887, NNG04G055G, and NAG5-13332, by the NSF under grant ATM-0455729. We also wish to thank the Swedish National Space Board for their support of the main PI institute and we are indebted to ESA for their courage in embarking on the Mars Express program.

## References

- Acuña, M. H., et al., Magnetic field and plasma observations at Mars: Initial results of the Mars Global Surveyor Mission, *Science*, 279, 1676, 1998.
- Arkani-Hamed, J., A 50-degree spherical harmonic model of the magnetic field of Mars, *J. Geophys. Res.*, 106, 23,197, 2001.
- Arkani-Hamed, J., An improved 50-degree spherical harmonic model of the magnetic field of Mars derived from both high-latitude and low-latitude data, *J. Geophys. Res.*, 107(E10), 5083, doi: 10.1029/2001JE001835, 2002.
- Barabash, S., et al., ASPERA-3: Analyser of space plasmas and energetic ions for Mars Express, in *Mars Express: The Scientific Payload*, ed. A. Wilson, European Space Agency Publications Division, European Space Research and Technology Centre, Noordwijk, The Netherlands, SP-1240, pp. 121-139, 2004.
- Chicarro, A., P. Martin, and R. Trautner, The Mars Express mission: An overview, in *Mars Express: The Scientific Payload*, ed. A. Wilson, European Space Agency Publications Division, European Space Research and Technology Centre, Noordwijk, The Netherlands, SP-1240, pp. 3-13, 2004.
- Connerney, J. E. P., M. H. Acuña, P. J. Wasilewski, G. Kleteschka, N. F. Ness, H. Rème, R. P. Lin, and D. L. Mitchell, The global magnetic field of Mars and implications for crustal evolution, *Geophys. Res. Lett.*, 28, 4015, 2001.
- Crider, D. H., et al., Observations of the latitude dependence of the location of the Martian magnetic pileup boundary, *Geophys. Res. Lett.*, 29(8), 1170, doi: 10.1029/2001GL013860, 2002.
- Frahm, R. A., et al., Carbon dioxide photoelectron peaks at Mars, *Icarus*, in press, 2006a.
- Frahm, R., et al., Locations of atmospheric photoelectron energy peaks within the Mars environment, *Space Sci. Rev.*, submitted, 2006b.

- Hanson, W. B., S. Sanatani, and D. R. Zuccaro, The Martian ionosphere as observed by the Viking retarding potential analyzers, *J. Geophys. Res.*, 82, 4351, 1977.
- Khazanov, G. V., and M. W. Liemohn, Nonsteady state ionosphere-plasmasphere coupling of superthermal electrons, *J. Geophys. Res.*, 100, 9669, 1995.
- Khazanov, G. V., M. W. Liemohn, J. U. Kozyra, and T. E. Moore, Inner magnetospheric superthermal electron transport: Photoelectron and plasma sheet electron sources, *J. Geophys. Res.*, 103, 23,485, 1998.
- Khazanov, G. V., M. W. Liemohn, J. U. Kozyra, and D. L. Gallagher, Global energy deposition to the topside ionosphere from superthermal electrons, *J. Atmos. Solar-Terr. Physics*, 62, 947, 2000.
- Lejeune, J., and F. Wörmsler, Diffusion of photoelectrons along a field line inside the plasmasphere, *J. Geophys. Res.*, 97, 159, 1992.
- Liemohn, M. W., et al., Numerical interpretation of high-altitude photoelectron observations, *Icarus*, 182, 383-395, 2006.
- Luhmann, J. G., and L. H. Brace, Near-Mars space, *Rev. Geophys.*, 29, 121, 1991.
- Ma, Y., A. F. Nagy, K. C. Hansen, D. L. DeZeeuw, and T. I. Gombosi, Three-dimensional multispecies MHD studies of the solar wind interaction with Mars in the presence of crustal fields, *J. Geophys. Res.*, 107(A10), 1282, doi: 10.1029/2002JA009293, 2002.
- Ma, Y., A. F. Nagy, I. V. Sokolov, and K. C. Hansen, Three-dimensional, multispecies, high spatial resolution MHD studies of the solar wind interaction with Mars, *J. Geophys. Res.*, 109, A07211, doi: 10.1029/2003JA010367, 2004.
- Mitchell, D. L., et al., Probing Mars' crustal magnetic field and ionosphere with the MGS electron reflectometer, *J. Geophys. Res.*, 106(E10), 23,419, 2001.
- Nagy, A. F., and P. M. Banks, Photoelectron flux in the Earth's ionosphere, *J. Geophys. Res.*, 75, 6260, 1970.
- Powell, K. G., P. L. Roe, T. J. Linde, T. I. Gombosi, D. L. De Zeeuw, A solution-adaptive upwind scheme for ideal magnetohydrodynamics, *J. Comp. Phys.*, 153, 284, 1999.

Schunk, R. M., and A. F. Nagy, *Ionospheres*, Cambridge University Press, New York, 2000.

Swartz, W. E., G. J. Bailey, and R. J. Moffett, Electron heating resulting from interhemispherical transport of photoelectrons, *Planet. Space Sci.*, *23*, 589, 1975.

Vennerstrom, S., N. Olsen, M. Purucker, M. H. Acuña, and J. C. Cain, The magnetic field in the pile-up region at Mars, and its variation with the solar wind, *Geophys. Res. Lett.*, *30*(7), 1369, doi: 10.1029/ 2003GL016883, 2003.

**Figure 1**

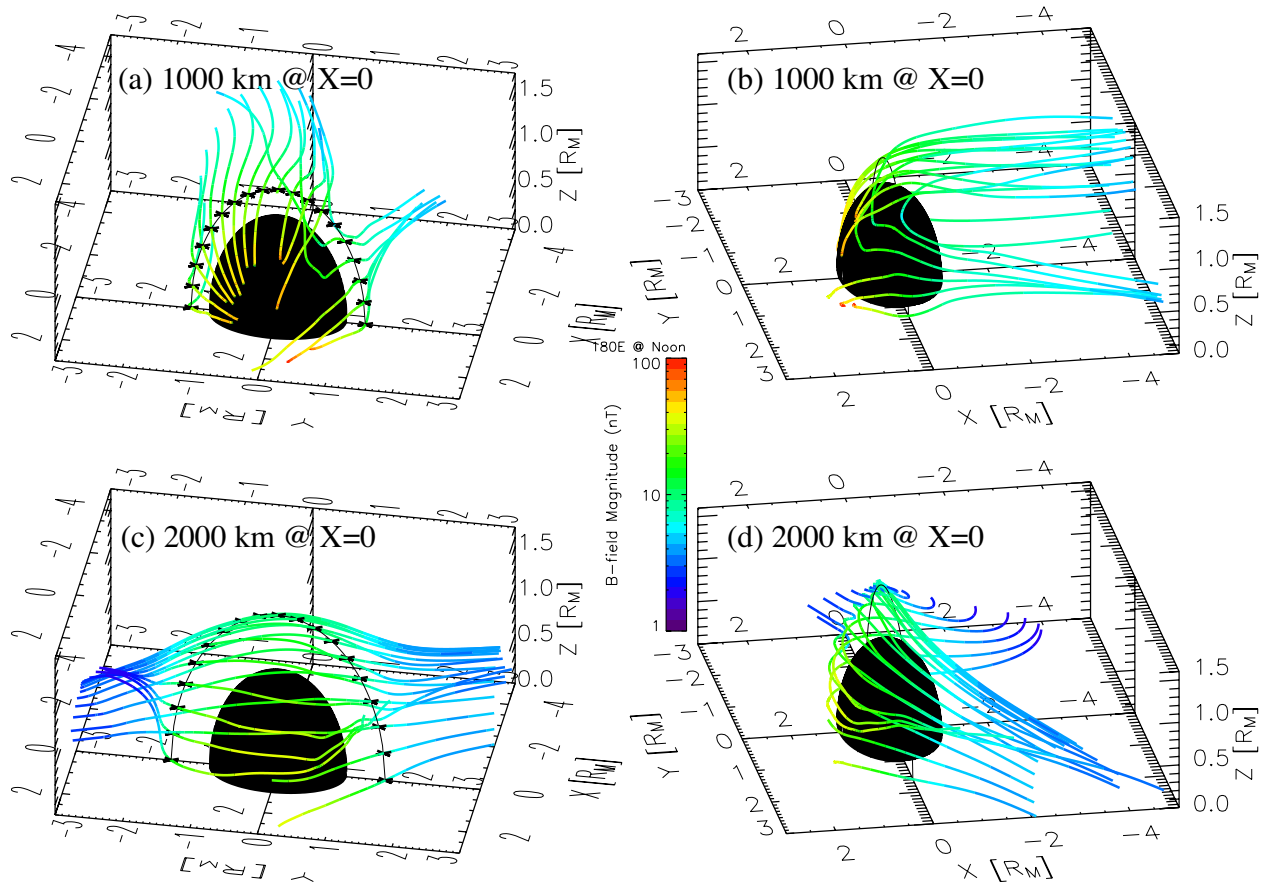


**Figure 1.** Field lines around Mars extracted from an MHD simulation, taken every  $10^\circ$  in a ring in the terminator plane ( $X=0$ ) at an altitude of (a and b) 1000 km and (c and d) 2000 km. The view in (a) and (c) is from the Sun, slightly above and to the right of the Sun-Mars line, while the view in (b) and (d) is from the dusk side, slightly above and to the left of the  $+y$  axis. The color shows the magnetic field magnitude along the field lines (log scale), the thin black circle shows the ring of positions from which the extractions began, and the black crosses in (a) and (c) show the starting points of the field line traces. The black hemisphere in the middle of each panel represents Mars.

**Figure 2**

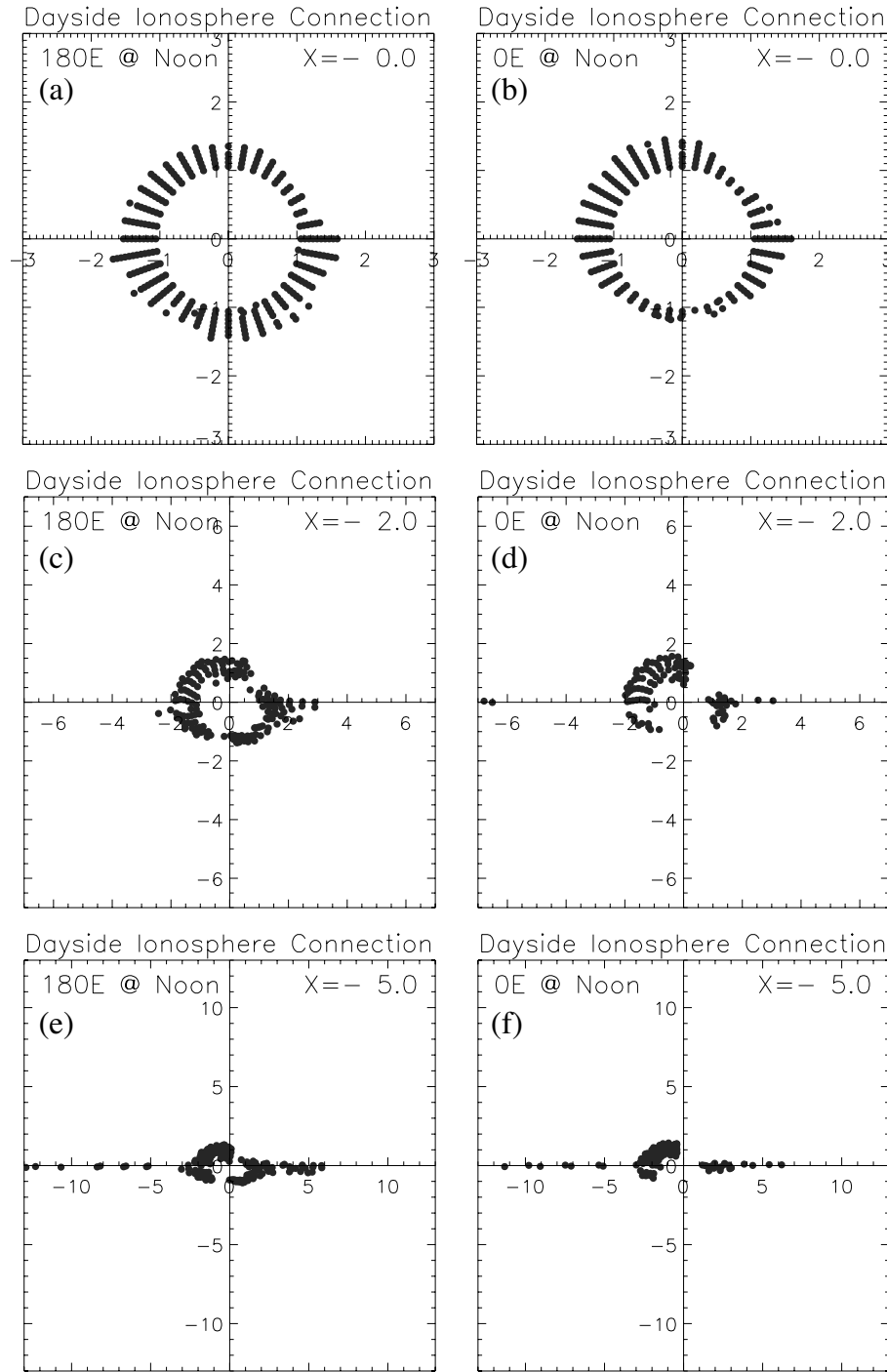


**Figure 2.** The y-z plane at (a and b)  $X=0$ , (c and d)  $X=-2$ , and (e and f)  $X=-5 R_M$  showing points of magnetic field connectivity to the dayside ionosphere for the simulation with subsolar longitude of (left column) 180E and (right column) 0E (strong crustal field toward and away from the Sun, respectively).

**Figure 3**

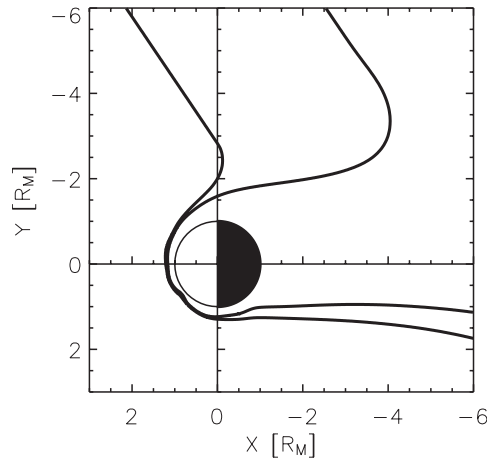


**Figure 3.** Two examples of S-shaped field lines that cross the  $x=0$  terminator plane three times.

**Figure 4**

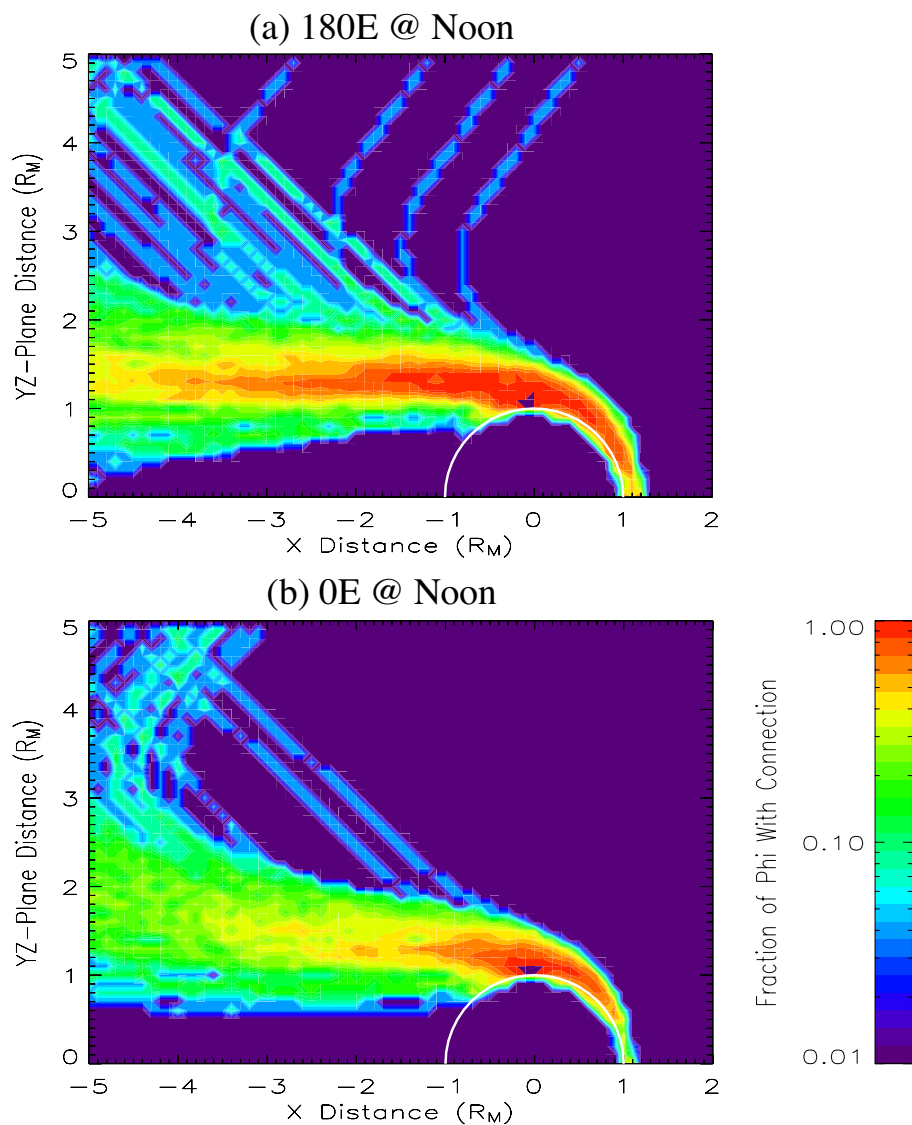


**Figure 4.** Fraction of field lines that have magnetic connectivity to the dayside ionosphere as a function of x distance and cylindrical distance from the x axis for the simulation with subsolar longitude of (a) 180E and (b) 0E. Note the logarithmic color scale.

**Figure 5**

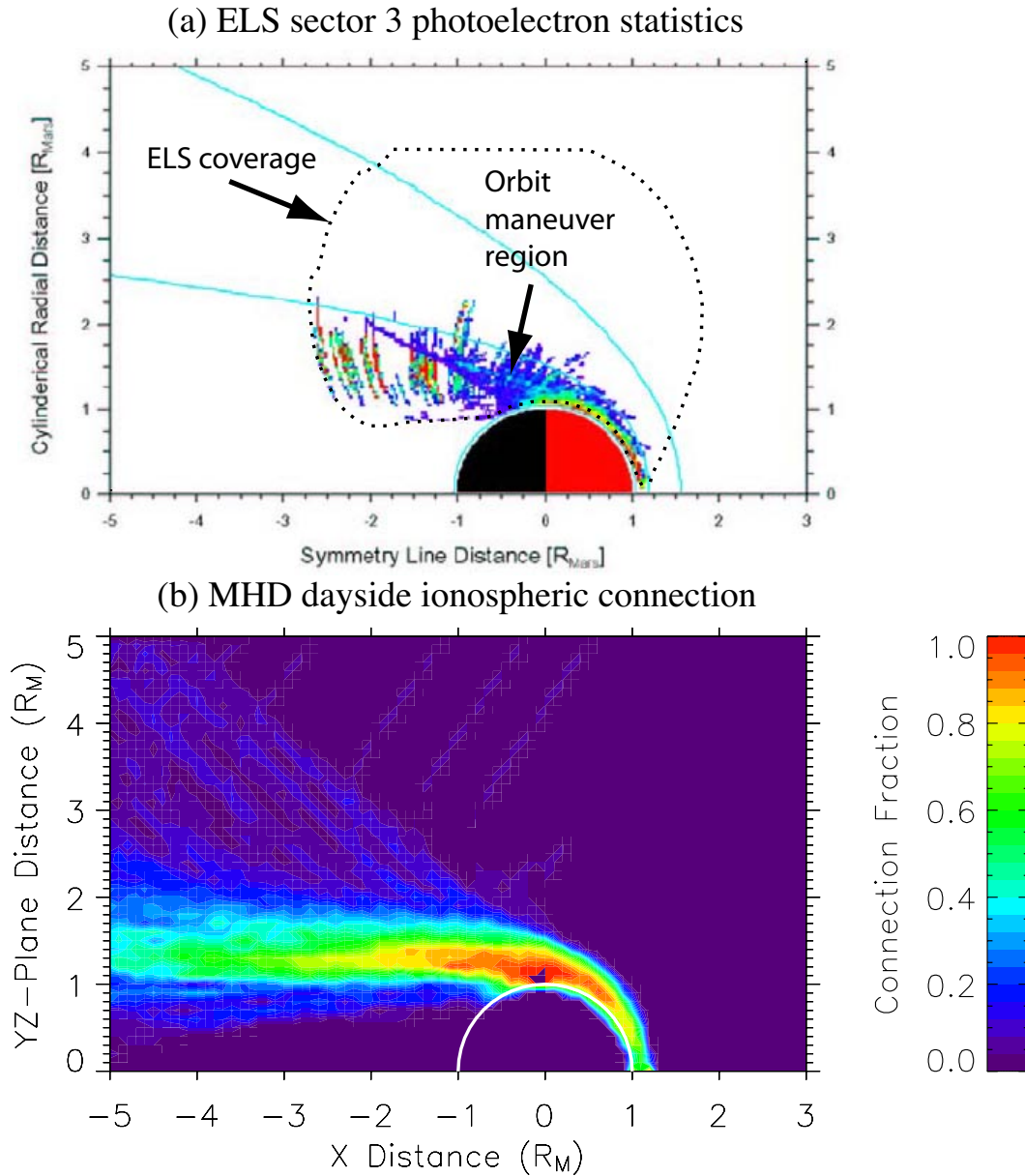


**Figure 5.** Measures of dayside ionospheric connectivity from the ELS instrument and the MHD model results, as a function of  $x$  distance and cylindrical distance from the  $x$  axis. (a) Fraction of ELS spectra containing atmospheric photoelectrons in sector 3 [from *Frahm et al.*, 2006b]. The black dotted line shows the region of ELS coverage included in the statistical analysis, and the two blue curves show the statistical locations of the magnetopause and bow shock. (b) Fraction of MHD field lines with connectivity, averaging the fractions from the 2 simulations. Note the linear color scale, which is the same for both plots.